Article

Limited increases in savanna carbon stocks over decades of fire suppression

https://doi.org/10.1038/s41586-022-04438-1

Received: 24 June 2021

Accepted: 14 January 2022

Published online: 16 March 2022

Check for updates

Yong Zhou[1,2]✉, Jenia Singh[3], John R. Butnor[4], Corli Coetsee[5,6], Peter B. Boucher[3], Madelon F. Case[2,7], Evan G. Hockridge[3], Andrew B. Davies[3] & A. Carla Staver[1,2]✉

Savannas cover a fifth of the land surface and contribute a third of terrestrial net primary production, accounting for three-quarters of global area burned and more than half of global fire-driven carbon emissions[1–3]. Fire suppression and afforestation have been proposed as tools to increase carbon sequestration in these ecosystems[2,4]. A robust quantification of whole-ecosystem carbon storage in savannas is lacking however, especially under altered fire regimes. Here we provide one of the first direct estimates of whole-ecosystem carbon response to more than 60 years of fire exclusion in a mesic African savanna. We found that fire suppression increased whole-ecosystem carbon storage by only 35.4 ± 12% (mean ± standard error), even though tree cover increased by 78.9 ± 29.3%, corresponding to total gains of 23.0 ± 6.1 Mg C ha^{-1} at an average of about 0.35 ± 0.09 Mg C ha^{-1} $year^{-1}$, more than an order of magnitude lower than previously assumed[4]. Frequently burned savannas had substantial belowground carbon, especially in biomass and deep soils. These belowground reservoirs are not fully considered in afforestation or fire-suppression schemes but may mean that the decadal sequestration potential of savannas is negligible, especially weighed against concomitant losses of biodiversity and function.

Savannas cover around 20% of the Earth's land surface and contribute to about 30% of terrestrial net primary production[2]. Fire-prone savannas represent one of the main sources of interannual variability in global atmospheric CO_2, as fire can change the sign of carbon fluxes at regional scales from year to year. It is estimated that tropical savannas account for about 71% of global burned area[1] and about 62% of global fire-driven carbon emissions[3]. As a result, fire suppression has been proposed as a tool to increase carbon sequestration[2,5] and savannas have been targeted by afforestation schemes promising to mitigate climate change[4]. Whether these schemes materialize or not, savannas are already burning less than they did historically[6], a pattern predicted by models to feed back to gains in carbon[7]. However, we lack any robust, direct quantifications of whole-ecosystem carbon storage in savannas that would allow us to rigorously evaluate their potential as a carbon sink, especially under altered fire regimes.

On the one hand, more frequent fires in savannas directly volatilize aboveground vegetation biomass carbon (including grasses, leaf litter and small trees and shrubs)[8]. This fire-driven efflux of carbon has measurable impacts on tree cover[9,10] and soil carbon[8], which — in turn — have been used as justification for the assumption that savannas store less carbon than their potential[2,4,5].

On the other hand, belowground carbon — especially in root biomass and subsurface soil pools — is rarely explicitly quantified in evaluations of fire effects on savanna whole-ecosystem carbon storage. Fire has well-documented impacts on soil carbon in surface layers[8], but carbon in subsurface soil layers is thought to be centuries old[11] and, therefore, may respond differently. In the few studies that consider belowground biomass[12,13], belowground biomass is arbitrarily assumed to increase in proportion to aboveground biomass, yielding constant root-to-shoot ratios across fire frequencies. However, this assumption is problematic: species-level root-to-shoot ratios vary across an order of magnitude for savanna trees[14], with much larger belowground allocation among savanna trees experiencing more frequent fires[15,16] (Extended Data Fig. 1). This bias probably yields biomass carbon estimates in frequently burned savannas that are too small and suggests that direct estimates of belowground carbon are needed for a complete account of whole-ecosystem carbon storage in savannas.

A further complication is that factors other than fire also determine savanna-ecosystem carbon stocks, and the magnitude of their effects compared with those of fire is unknown. At regional to continental scales, rainfall systematically increases aboveground carbon and maximum potential tree cover[10,17]. At local scales, differences in soil texture can have substantial effects on tree cover, the depth distribution of root biomass and soil carbon[18,19].

A comprehensive understanding of savanna whole-ecosystem carbon storage requires rigorous and direct empirical evaluation. Here we used a long-term burning experiment in Kruger National Park, South Africa (Extended Data Fig. 2) to examine how changes in fire frequency affect savanna carbon storage and allocation in vegetation and soil. This experiment, initiated in 1954, is one of the longest running in Africa. We focused on the four wettest replicates (in Pretoriuskop), with mean annual rainfall of roughly 700 mm (Extended Data Fig. 2),

[1]Yale Institute for Biospheric Studies, Yale University, New Haven, CT, USA. [2]Department of Ecology and Evolutionary Biology, Yale University, New Haven, CT, USA. [3]Department of Organismic and Evolutionary Biology, Harvard University, Cambridge, MA, USA. [4]USDA Forest Service, Southern Research Station, University of Vermont, Burlington, VT, USA. [5]Scientific Services, SANParks, Skukuza, South Africa. [6]School of Natural Resource Management, Nelson Mandela University, George, South Africa. [7]Present address: Institute of Ecology and Evolution, University of Oregon, Eugene, OR, USA. ✉e-mail: yong.zhou@yale.edu; carla.staver@yale.edu

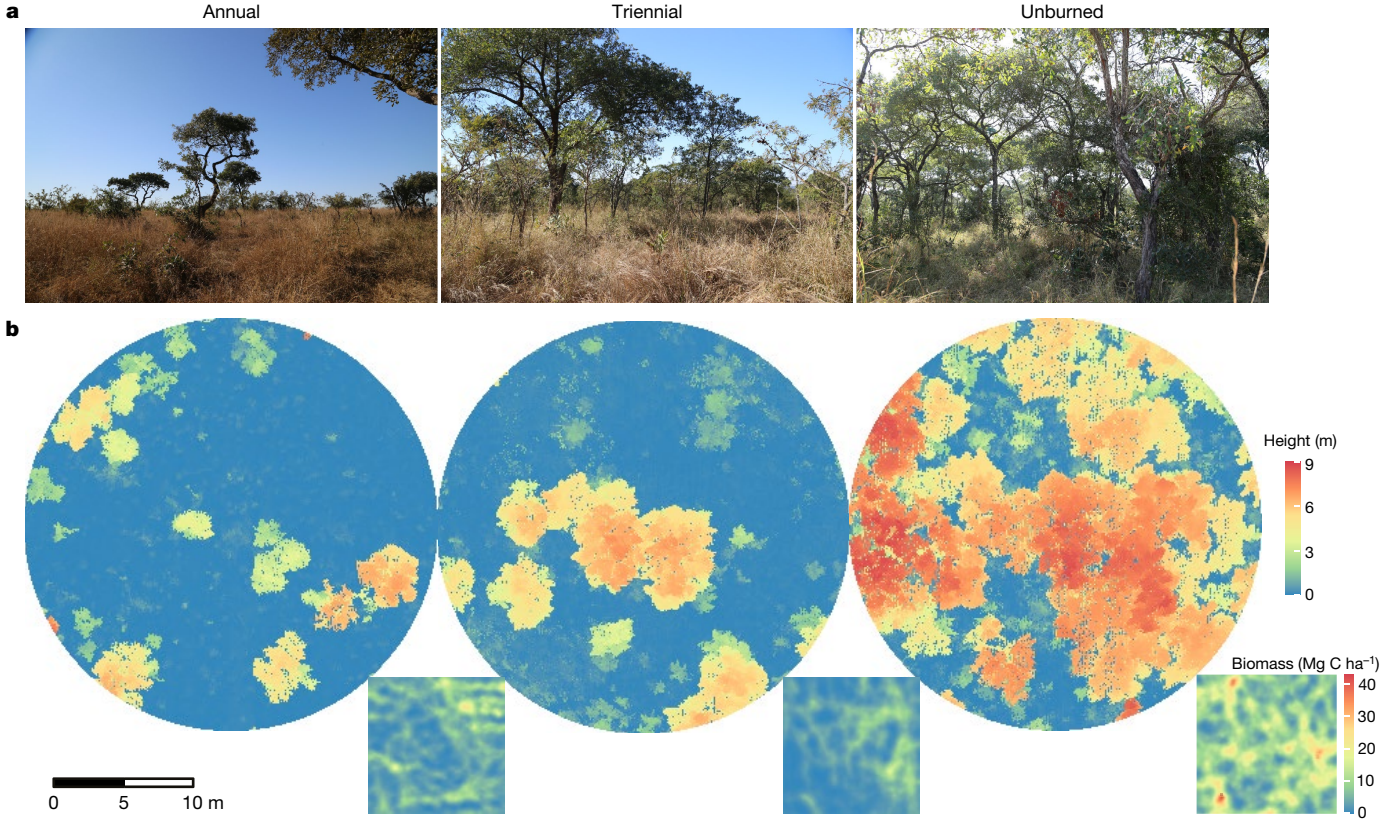

Fig. 1 | Vegetation characteristics of experimental burn plots in a mesic savanna in Kruger National Park, South Africa. a, Example pictures showing vegetation structure in different fire treatments. **b**, Examples of tree canopy cover and height (that is, 30-m-diameter circular plots) derived from airborne light detection and ranging and belowground coarse-root biomass (that is, 10 × 10-m square plots) estimated from ground-penetrating radar in different fire treatments. The 10 × 10-m plots are roughly located at the centre of the 30-m-diameter plots. See Supplementary Figs. 1–4 for all treatment replicates with enlarged images.

because they were the most likely to show increases in tree cover and whole-ecosystem carbon storage with fire exclusion[9] (noting that drier savannas also merit direct consideration). We sampled a subset of fire treatments: an extreme scenario with fires every August (that is, dry-season annual burning), a near-natural landscape average[20] with fires every three years in August (that is, triennial burning) and an unburned treatment subjected to more than six decades of fire suppression.

Recent advances in remote sensing are improving the accuracy and extent of vegetation biomass estimation. Aboveground, light detection and ranging (LiDAR) provides extensive, high-resolution maps of savanna woody biomass[21,22]. Belowground, techniques are comparatively in their infancy, but some hold promise for alleviating the intensive labour required to excavate and quantify root biomass directly. Specifically, ground-penetrating radar (GPR), supplemented with field calibrations to improve accuracy, offers a non-destructive method for quantifying coarse-root biomass at fine scales[23]. At each treatment replicate, we established one 10 × 10-m GPR plot for estimating coarse lateral-root biomass to a depth of 60 cm (Fig. 1, Supplementary Figs. 1–4). Because GPR methods are better at quantifying lateral coarse roots than taproots, we supplemented GPR measurements with woody taproot biomass estimated by means of a site-specific diameter at breast height (DBH) allometry (Supplementary Fig. 5). We also used a core-sampling method to estimate fine-root biomass and soil organic carbon (SOC) to a depth of 60 cm, which were further partitioned into C_3 (woody plant) versus C_4 (grass) contributions on the basis of stable carbon isotope mixture methods (Extended Data Fig. 3). Aboveground woody biomass was estimated using high-resolution, drone-based LiDAR within 15 m of the centre of each GPR plot (to allow for small location errors; Fig. 1, Supplementary Figs. 1–4). Because measurements of herbaceous biomass using LiDAR are not yet reliable, we used long-term fuel-load monitoring data to estimate aboveground grass biomass (Extended Data Fig. 4).

We found that less frequent fires substantially increased tree height, tree cover, and aboveground woody biomass (Fig. 2a, Extended Data Table 1, Supplementary Table 1), consistent with previous work[12,13]. Compared with triennial burning, fire suppression increased tree height, tree cover, and aboveground woody biomass by 32% (standard error, se = 15%, $n = 4$), 79% (se = 29%) and 157% (se = 79%), respectively, whereas annual burning decreased these by 6% (se = 10%), 22% (se = 19%) and 34% (se = 21%), respectively. Less frequent fires also increased aboveground grass biomass (Fig. 2a, Extended Data Table 1). However, the contribution of grasses to total standing aboveground biomass was small (about 10%) and temporally variable (Fig. 2a, Extended Data Fig. 4), largely driven by interannual rainfall variability[24].

Less frequent fires also increased woody fine, coarse lateral, and taproot biomass (Fig. 2a, Extended Data Table 1), confirming that increasing tree cover also increased belowground woody biomass[25]. However, belowground increases were not proportional to aboveground increases, and annually burned savannas had higher root-to-shoot ratios than those burned triennially or not burned (Fig. 2b). This result contradicts the assumption of constant root-to-shoot ratio applied elsewhere to estimate belowground carbon[12,13] but agrees with evidence that trees in frequently burned savannas invest heavily in belowground carbon for post-fire recovery[15,16] (Extended Data Fig. 1). However, a robust quantification of belowground biomass always remains a great challenge in terms of methodology, accuracy, and efficiency in savannas and other ecosystems, and our estimates also carry some

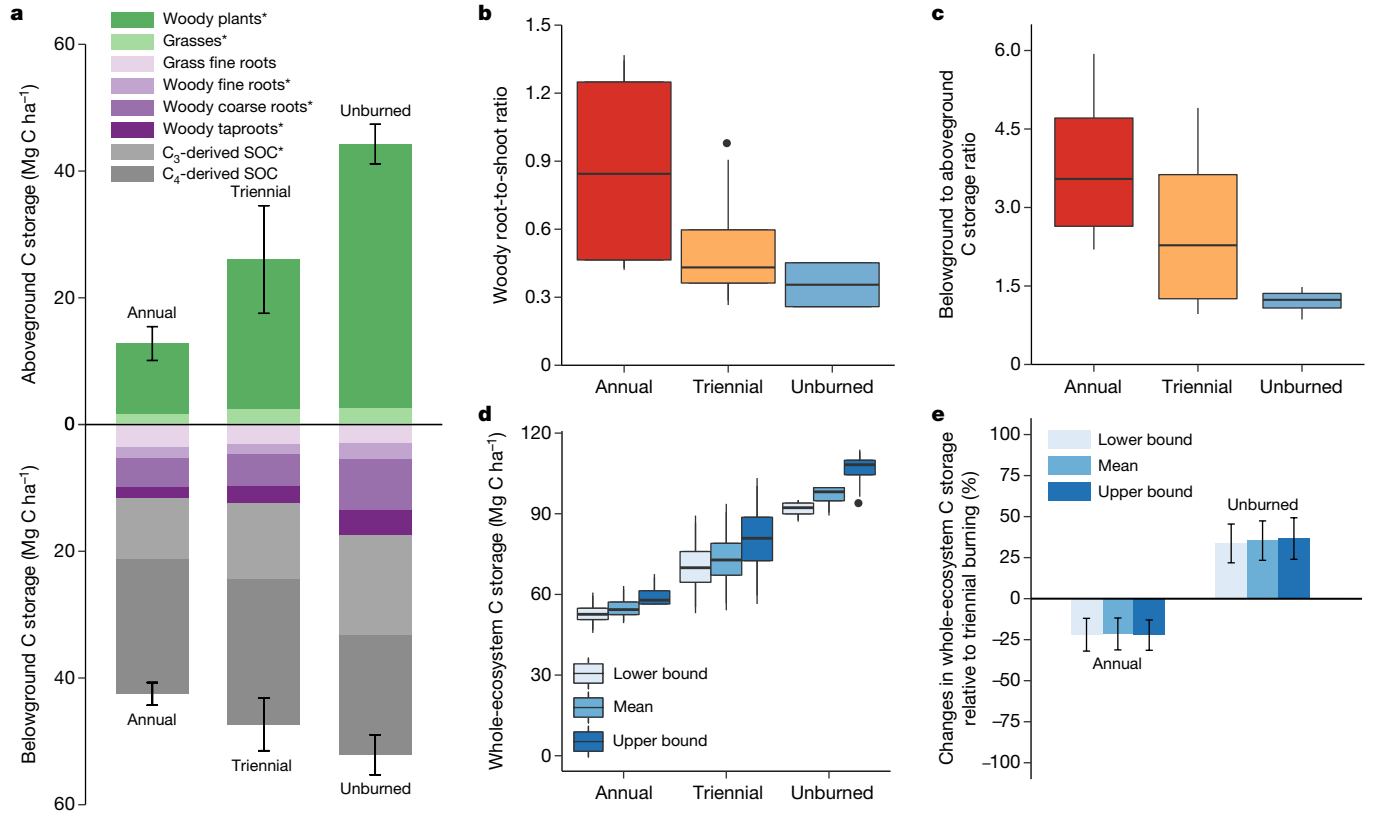

Fig. 2 | Changes in whole-ecosystem carbon storage across fire treatments. **a**, Carbon storage estimated across different aboveground and belowground pools. C_3-derived SOC is from woody plants, whereas C_4-derived SOC is from grasses. Values for each C pool are means of four replicates (see Supplementary Table 2). Carbon pools with * indicate notable influence of fire treatments at the level of $P < 0.05$ on the basis of linear mixed models or ranked mixed models (see Extended Data Table 1). **b**, **c**, Changes in woody root-to-shoot ratio and ratio of belowground to aboveground C storage across different fire treatments. **d**, The uncertainty of whole-ecosystem carbon storage across different fire treatments. The uncertainty is derived from different scenarios of coarse lateral and taproot biomass estimates (lower bound, mean, upper bound) (see Extended Data Fig. 5). **e**, Changes in whole-ecosystem carbon storage relative to triennial burning (%). The box plots show medians (that is, 50th percentile), 25th and 75th percentiles, and 95% confidence intervals of four replicates. Points in **b** and **d** indicate outliers. Error bars in **a** and **e** indicate standard errors ($n = 4$).

uncertainty. Plot-level coarse-lateral-root biomass estimated from GPR was highly correlated with taproot biomass estimated from DBH ($R^2 = 0.75$) (Extended Data Fig. 5a), cross-validating the assessments by means of the two methods. Despite this, biomass estimates from lower and higher bounds of the 95% confidence intervals differed up to three-fold (Extended Data Fig. 5). However, the magnitude of uncertainty was comparable across fire treatments (Fig. 2d, Extended Data Fig. 5) and, therefore, relative changes in whole-ecosystem carbon storage owing to fire suppression were much more consistent (mean = 35.4%, 95% confidence interval = 33.6 to 36.6%) (Fig. 2e).

Theoretically, frequent or severe fires produce heat that can readily kill roots in surface soils[26], such that trees in frequently burned savannas might allocate roots to deeper soil profiles. However, variation in the depth distribution of GPR detections (as a surrogate for rooting depth) did not support this hypothesis (Extended Data Fig. 6). Although savanna trees experiencing annual fires rooted marginally deeper than those burned infrequently, these differences were far from important. However, we found strong support for the hypothesis that savanna trees root deeper on sandier soils ($R^2 = 0.61$) (Extended Data Fig. 6), where water percolates more readily and mechanical impedance to root penetration is lower[19,27]. The application of GPR to examine depth distributions of root biomass may provide further opportunity to explore functional rooting depth of savanna trees and associated ecological questions around tree–grass competition.

We found that changes in fire frequencies did not affect total SOC storage (Fig. 2a, Extended Data Table 1), although SOC trended slightly higher with less frequent fires. At first glance, this result seems to contradict work showing that fire suppression increases soil carbon storage[8], because SOC is higher under tree canopies[28,29]. However, most previous work in savannas has only sampled soils to a very shallow depth (for example, 0–20 cm)[8], whereas we integrated SOC throughout the soil column to represent total SOC. When we re-evaluated past findings from the same site for fire effects on total SOC including deeper soils[28], we found results consistent with what we report here: fire suppression had unimportant effects on total SOC across the soil column, because differences were restricted to shallow soil layers[28] (Supplementary Fig. 6). Deep soil carbon is clearly a neglected carbon pool.

Our results challenge the assumption that systems without trees are impoverished in soil carbon[4]. Instead, it is clear that savannas, like most terrestrial ecosystems, store substantial carbon in soils even in treeless areas[2]. Indeed, grass net primary productivity in tropical savannas is comparable with and even higher than tree productivity[30], and the inputs of C_4-derived carbon into soils can be an important source of SOC[31]. For example, we found that less frequent fires increased C_3 (woody)-derived SOC (Fig. 2a), which scaled positively with increasing tree cover ($R^2 = 0.68$) (Fig. 3c), but that C_4 (grass)-derived carbon dominated SOC even at around 80% tree cover in the unburned treatment (Fig. 2a), especially in deeper soil profiles (Extended Data Fig. 3). In part, this is probably driven by the slow turnover of deep-soil carbon[11,32], which suggests that management on decadal or even century scales may have relatively small effects on soil carbon. However, even at equilibrium, SOC may not increase proportionally with increasing

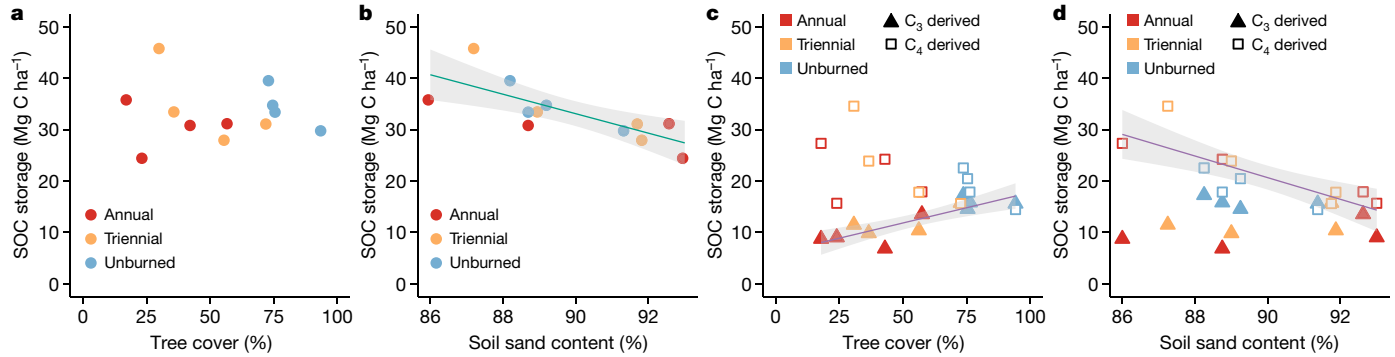

Fig. 3 | Changes in SOC with tree cover and soil sand content. Total SOC storage does not change with tree cover ($R^2 = 0.00$, $P = 0.95$) (**a**) but decreases with soil sand content ($R^2 = 0.56$, $P = 0.004$) (**b**). C_3-derived SOC increases with tree cover ($R^2 = 0.68$, $P = 0.001$) but C_4-derived SOC does not ($R^2 = 0.21$, $P = 0.08$) (**c**). C_4-derived SOC decreases with soil sand content ($R^2 = 0.63$, $P = 0.001$) but C_3-derived SOC does not ($R^2 = 0.02$, $P = 0.67$) (**d**). Regression lines indicate significant linear fits and shaded bands illustrate the 95% confidence interval of the linear fit.

tree cover (or woody biomass) (Fig. 3a), as soils can be subject to carbon saturation depending on soil texture and mineralogy. Sandy soils have much less physical protection for SOC and thus lower saturation thresholds compared with clayey soils[33]. Here we found that C_4-derived ($R^2 = 0.63$) and total SOC ($R^2 = 0.56$) decreased with subtle variation in soil sand content (Fig. 3b, d) but not fire frequency.

Integrating across all pools, more carbon was stored belowground than aboveground across all fire treatments (Fig. 2a). Both fire suppression and increasing tree cover increased the amount of carbon stored belowground (Fig. 2a), but increases were variable, and belowground carbon increased much less and less consistently than aboveground carbon with fire suppression (Fig. 2c, Extended Data Table 1). As a result, the ratio of belowground to aboveground carbon storage actually decreased with increasing tree cover ($R^2 = 0.83$) (Extended Data Fig. 7), further challenging the assumption that savannas with sparse tree cover have limited or no belowground carbon storage[4]. Almost 85% of whole-ecosystem carbon was stored belowground when tree cover was <20% in this savanna (Extended Data Fig. 7). Savannas clearly have substantial belowground carbon pools.

Taken together, our results indicate that less frequent fires increased whole-ecosystem carbon storage in this savanna (Fig. 2a, d, Extended Data Table 1). Increased carbon storage is mainly attributable to increased aboveground woody biomass (Fig. 2a), consistent with previous work in savannas[28,29]. However, increases in carbon storage are smaller at the level of the whole ecosystem than sometimes assumed. Compared with triennial burning, six decades of fire suppression increased whole-ecosystem carbon storage by only 35.4% (se = 12.0%, $n = 4$), whereas annual burning decreased it by only 21.5% (se = 9.7%, $n = 4$) (Fig. 2e). Across six decades, fire-suppressed savannas sequestered 23.0 Mg C ha^{-1} (se = 6.1 Mg C ha^{-1}, $n = 4$) more carbon than savannas experiencing near-natural, triennial burning, amounting to an annual carbon sequestration rate of about 0.35 Mg C ha^{-1} year^{-1}. This is a time-averaged estimate, which may mask some non-linearities, especially in the rate of aboveground biomass accumulation. However, our estimate is similar in magnitude to the 0.14 Mg C ha^{-1} year^{-1} documented in a synthesis of global tropical savanna productivity[2]. By contrast, studies using space-for-time substitutions to estimate carbon sequestration rates, with treeless savannas and closed-canopy forests as end points, instead report rates ranging from 1.2 to 1.8 Mg C ha^{-1} year^{-1} (refs. [13,34]) — a clear overestimate. This discrepancy arises simply because these studies neglect belowground savanna carbon pools and ignore the timescales of transition from savanna to closed-canopy forest.

Overall, we argue that increasing tree cover in savannas, whether by means of afforestation or fire suppression, is unlikely to yield the substantial gains in ecosystem carbon storage that have been advertised. For example, a recent report suggested that reforesting a billion hectares of Earth's land surface could store a massive 205 gigatonnes of carbon (GtC)[4], with the largest sequestration potential located in tropical grassy ecosystems including savannas (about 190 million hectares; about 53.5 GtC of sequestration potential). These estimates rely on ecosystem carbon gains totalling 283 Mg C ha^{-1} from increasing tree densities, a modelled estimate that is 12 times higher than our empirical estimate. Moreover, existing estimates assume that potential sequestration will be achieved before the year 2050 (over <30 years, at an annual rate of about 9.4 Mg C ha^{-1} year^{-1}), whereas we observed a smaller gain rate over a total of 65 years (at an annual rate of about 0.35 Mg C ha^{-1} year^{-1}, a number that is 27 times smaller). Although further study is needed, especially in savannas in more humid environments (which are more productive) and on more clayey soils (which may store relatively more carbon in slow-turnover soil pools), it is clear that arbitrarily applying carbon densities observed in tropical forests to estimate carbon gains of tropical grassy ecosystems represents a massive overestimate of the carbon sequestration value of fire suppression and afforestation. Leaving aside the influence of afforesting savannas on biodiversity, ecosystem function and socioecological value[34,35], it is obvious that the carbon benefits of increasing woody biomass in savanna ecosystems have been grossly overstated.

This work also highlights the importance of chronically disturbed, open-canopy ecosystems for long-term carbon storage in the Earth system. The concept of 'avoided deforestation' has become a key talking point in discussions about the potential contributions of nature-based solutions for climate mitigation[36], but no such equivalent framing has been applied to savannas and other grassy ecosystems. Even today, natural and managed savannas cover about 20% of global land area but are poorly protected and increasingly threatened by land-use conversions[37]. Trees-for-carbon schemes are included in this threat. That these systems contain substantial and slow-turnover carbon stocks, especially belowground, emphasizes the urgent need to consider explicitly — and to protect — their substantial existing contributions to carbon storage.

Continuing human-driven changes in fire regimes, in parallel with changing land use, atmosphere and climate, probably have large impacts on savanna ecosystems. To evaluate how these impacts will shape ecosystem carbon storage, long-term experimental and empirical datasets will be critical. Possible climate-change-associated expansion of drylands across the tropics[38] make this need all the more urgent. Our results provide robust evidence of limited savanna carbon gains from increasing tree cover when fire is suppressed for more than six decades, suggesting that the benefits of trees-for-carbon and fire-suppression schemes for climate mitigation have been exaggerated. The experiment and dataset presented here are rare and previously unknown in tropical savannas, and work such as this must be applied more broadly.

Robust quantifications of carbon sequestration must also be considered alongside the potential negative impacts of afforestation and fire suppression on biodiversity at all trophic levels[34,39] and on other ecosystem functions (including grazing[40], hydrologic cycles[41] and – in some systems – extreme fire risk[42]). This context makes our results especially alarming: overestimating carbon gains from increasing tree cover offers false promise for climate mitigation, at a very real cost to biodiversity and ecosystem function.

Online content

Any methods, additional references, Nature Research reporting summaries, source data, extended data, supplementary information, acknowledgements, peer review information; details of author contributions and competing interests; and statements of data and code availability are available at https://doi.org/10.1038/s41586-022-04438-1.

1. Giglio, L., Schroeder, W. & Justice, C. O. The collection 6 MODIS active fire detection algorithm and fire products. *Remote Sens. Environ.* **178**, 31–41 (2016).
2. Grace, J., José, J. S., Meir, P., Miranda, H. S. & Montes, R. A. Productivity and carbon fluxes of tropical savannas. *J. Biogeogr.* **33**, 387–400 (2006).
3. Van Der Werf, G. R. et al. Global fire emissions estimates during 1997–2016. *Earth Syst. Sci. Data* **9**, 697–720 (2017).
4. Bastin, J.-F. et al. The global tree restoration potential. *Science* **365**, 76–79 (2019).
5. Russell-Smith, J. et al. Opportunities and challenges for savanna burning emissions abatement in southern Africa. *J. Environ. Manage.* **288**, 112414 (2021).
6. Andela, N. et al. A human-driven decline in global burned area. *Science* **356**, 1356–1362 (2017).
7. Wu, C. et al. Historical and future global burned area with changing climate and human demography. *One Earth* **4**, 517–530 (2021).
8. Pellegrini, A. F. A. et al. Fire frequency drives decadal changes in soil carbon and nitrogen and ecosystem productivity. *Nature* **553**, 194–198 (2018).
9. Higgins, S. I. et al. Effects of four decades of fire manipulation on woody vegetation structure in savanna. *Ecology* **88**, 1119–1125 (2007).
10. Staver, A. C., Archibald, S. & Levin, S. A. The global extent and determinants of savanna and forest as alternative biome states. *Science* **334**, 230–232 (2011).
11. Shi, Z. et al. The age distribution of global soil carbon inferred from radiocarbon measurements. *Nat. Geosci.* **13**, 555–559 (2020).
12. Pellegrini, A. F. A., Hedin, L. O., Staver, A. C. & Govender, N. Fire alters ecosystem carbon and nutrients but not plant nutrient stoichiometry or composition in tropical savanna. *Ecology* **96**, 1275–1285 (2015).
13. Tilman, D. et al. Fire suppression and ecosystem carbon storage. *Ecology* **81**, 2680–2685 (2000).
14. Mokany, K., Raison, R. J. & Prokushkin, A. S. Critical analysis of root:shoot ratios in terrestrial biomes. *Glob. Change Biol.* **12**, 84–96 (2006).
15. de Miranda, S. D. C. et al. Regional variations in biomass distribution in Brazilian savanna woodland. *Biotropica* **46**, 125–138 (2014).
16. Wigley, B. J., Cramer, M. D. & Bond, W. J. Sapling survival in a frequently burnt savanna: mobilisation of carbon reserves in *Acacia karroo*. *Plant Ecol.* **203**, 1 (2009).
17. Sankaran, M. et al. Determinants of woody cover in African savannas. *Nature* **438**, 846–849 (2005).
18. Staver, A. C., Botha, J. & Hedin, L. Soils and fire jointly determine vegetation structure in an African savanna. *New Phytol.* **216**, 1151–1160 (2017).
19. Zhou, Y., Wigley, B. J., Case, M. F., Coetsee, C. & Staver, A. C. Rooting depth as a key woody functional trait in savannas. *New Phytol.* **227**, 1350–1361 (2020).
20. Govender, N., Trollope, W. S. W., Van, & Wilgen, B. W. The effect of fire season, fire frequency, rainfall and management on fire intensity in savanna vegetation in South Africa. *J. Appl. Ecol.* **43**, 748–758 (2006).
21. Colgan, M. S., Asner, G. P. & Swemmer, T. Harvesting tree biomass at the stand level to assess the accuracy of field and airborne biomass estimation in savannas. *Ecol. Appl.* **23**, 1170–1184 (2013).
22. Davies, A. B. & Asner, G. P. Elephants limit aboveground carbon gains in African savannas. *Glob. Change Biol.* **25**, 1368–1382 (2019).
23. Butnor, J. R. et al. Utility of ground-penetrating radar as a root biomass survey tool in forest systems. *Soil Sci. Soc. Am. J.* **67**, 1607–1615 (2003).
24. Staver, A. C., Wigley-Coetsee, C. & Botha, J. Grazer movements exacerbate grass declines during drought in an African savanna. *J. Ecol.* **107**, 1482–1491 (2019).
25. Ryan, C. M., Williams, M. & Grace, J. Above- and belowground carbon stocks in a miombo woodland landscape of Mozambique. *Biotropica* **43**, 423–432 (2011).
26. Swezy, D. M. & Agee, J. K. Prescribed-fire effects on fine-root and tree mortality in old-growth ponderosa pine. *Can. J. For. Res.* **21**, 626–634 (1991).
27. Canadell, J. et al. Maximum rooting depth of vegetation types at the global scale. *Oecologia* **108**, 583–595 (1996).
28. Coetsee, C., Bond, W. J. & February, E. C. Frequent fire affects soil nitrogen and carbon in an African savanna by changing woody cover. *Oecologia* **162**, 1027–1034 (2010).
29. Holdo, R. M., Mack, M. C. & Arnold, S. G. Tree canopies explain fire effects on soil nitrogen, phosphorus and carbon in a savanna ecosystem. *J. Veg. Sci.* **23**, 352–360 (2012).
30. Lloyd, J. et al. Contributions of woody and herbaceous vegetation to tropical savanna ecosystem productivity: a quasi-global estimate. *Tree Physiol.* **28**, 451–468 (2008).
31. Wigley, B. J., Augustine, D. J., Coetsee, C., Ratnam, J. & Sankaran, M. Grasses continue to trump trees at soil carbon sequestration following herbivore exclusion in a semiarid African savanna. *Ecology* **101**, e03008 (2020).
32. Khomo, L., Trumbore, S., Bern, C. R. & Chadwick, O. A. Timescales of carbon turnover in soils with mixed crystalline mineralogies. *Soil* **3**, 17–30 (2017).
33. Six, J., Conant, R. T., Paul, E. A. & Paustian, K. Stabilization mechanisms of soil organic matter: implications for C-saturation of soils. *Plant Soil* **241**, 155–176 (2002).
34. Abreu, R. C. R. et al. The biodiversity cost of carbon sequestration in tropical savanna. *Sci. Adv.* **3**, e1701284 (2017).
35. Bond, W. J., Stevens, N., Midgley, G. F. & Lehmann, C. E. The trouble with trees: afforestation plans for Africa. *Trends Ecol. Evol.* **34**, 963–965 (2019).
36. West, T. A., Börner, J. & Fearnside, P. M. Climatic benefits from the 2006–2017 avoided deforestation in Amazonian Brazil. *Front. For. Glob. Change* **2**, 52 (2019).
37. Aleman, J. C., Blarquez, O. & Staver, C. A. Land-use change outweighs projected effects of changing rainfall on tree cover in sub-Saharan Africa. *Glob. Change Biol.* **22**, 3013–3025 (2016).
38. Huang, J., Yu, H., Guan, X., Wang, G. & Guo, R. Accelerated dryland expansion under climate change. *Nat. Clim. Change* **6**, 166–171 (2016).
39. Ratajczak, Z., Nippert, J. B. & Collins, S. L. Woody encroachment decreases diversity across North American grasslands and savannas. *Ecology* **93**, 697–703 (2012).
40. Smit, I. P. & Prins, H. H. Predicting the effects of woody encroachment on mammal communities, grazing biomass and fire frequency in African savannas. *PLoS One* **10**, e0137857 (2015).
41. Huxman, T. E. et al. Ecohydrological implications of woody plant encroachment. *Ecology* **86**, 308–319 (2005).
42. Hermoso, V., Regos, A., Morán-Ordóñez, A., Duane, A. & Brotons, L. Tree planting: a double-edged sword to fight climate change in an era of megafires. *Glob. Change Biol.* **27**, 3001–3003 (2021).

Methods

Study site

Kruger National Park (latitude: 22°20′–25°30′S; longitude: 31°10′–32°00′E) (hereafter, Kruger) is the largest protected area (around 20,000 km^2) in South Africa (Extended Data Fig. 2), consisting of subtropical and tropical savannas. Mean annual rainfall increases from 350 mm in the north part of Kruger to 750 mm in the south (Extended Data Fig. 2), with rainfall concentrated in the wet season between November and April. Kruger is dominated by two underlying parent materials, a granite (sandy and nutrient poor) and a basalt (clayey and nutrient rich), which have strong influences on vegetation[18,43]. Although the fire-return interval varies spatially across Kruger, the average is about 3.5 years (ref. [20]) The flora of Kruger includes >200 species of grasses and >400 species of trees and shrubs[43].

Experimental design

Kruger maintains one of a handful of long-term burning experiments in tropical savannas. The experimental burning plots (EBPs) were initiated in 1954, making them one of the longest-running fire ecology research projects in African savannas. The overall aim of the EBPs is to determine how fire frequency and season shape savanna vegetation structure and ecosystem functioning. The EBPs are distributed across four different landscapes of Kruger (that is, Mopani, Satara, Skukuza and Pretoriuskop), with different dominant tree species, parent materials and rainfall (Extended Data Fig. 2). Each landscape can be considered as an independent factorial design with four replicates (hereafter, strings). In each string, there are 12 treatments, with the fire-return interval of each treatment representing a different combination of frequency and season[9,44]. For this study, we selected the Pretoriuskop landscape receiving around 700 mm of rainfall (Extended Data Fig. 2), which broadly represents African savannas that have the potential to reach full tree cover[17]. Among these 12 treatments, we selected plots burned every year in August (hereafter, annual) to represent an extreme fire regime; plots burned every three years in August (hereafter, triennial) to represent the near-natural fire-return interval of African savannas[20]; and plots that have not burned since 1954 (hereafter, unburned) to represent savannas with fire-suppressed status.

At each treatment in each string across the Pretoriuskop landscape, we randomly established a 10 × 10-m plot for field measurement and sample collection in September 2018. We recorded the longitude and latitude coordinates of each plot. In each plot, we further recorded woody species identity, DBH (only those with DBH > 5 cm), height and x and y coordinates relative to the 10 × 10-m plot.

Soil carbon storage estimation

To estimate soil carbon storage, we randomly sampled four soil cores (7 cm in diameter) to a depth of 60 cm and separated into four soil layers (0–15, 15–30, 30–45 and 45–60 cm) in each 10 × 10-m plot. Soil samples were air-dried and passed through a 2-mm sieve. A subsample of sieved soils was further oven-dried at 65 °C and then ground to a fine powder with a mortar and pestle. An aliquot of ground soils was acid-washed to remove carbonate and then oven-dried at 65 °C. SOC concentrations and stable carbon isotopic values of acid-washed soils were determined using a Costech ECS 4010 elemental analyzer interfaced by means of a ConFlo III device with a Delta V Advantage isotope ratio mass spectrometer at the Yale Analytical and Stable Isotope Center. The stable isotopic values (δ^{13}C) were expressed as deviations from an international standard (that is, Vienna Pee Dee Belemnite) in parts per thousand (‰) using δ-notation:

$$\delta = \left[\left(\frac{R_{\text{sample}}}{R_{\text{standard}}} - 1\right) * 1,000\right] \quad (1)$$

in which R is the ratio of ^{13}C to ^{12}C isotope for sample and standard. The precision of duplicate measurements was 0.1‰.

As all grasses in this savanna are C_4 species, we further calculated the relative proportion of SOC derived from woody plants (f) and grasses ($1-f$) for each soil layer using a mass balance equation:

$$f = \frac{\delta_s - \delta_g}{\delta_w - \delta_g} \quad (2)$$

in which δ_s is the measured δ^{13}C value for soil samples, δ_w is the mean δ^{13}C value for woody plants and δ_g is the mean δ^{13}C value for grasses. We used −26.7‰ (n = 49 species) and −12.5‰ (n = 93 species) as the endmembers for woody plants and grasses, respectively, across the Pretoriuskop landscape[45]. Soil bulk density was determined for each soil layer from drying a known volume of undisturbed soils and used for calculating SOC storage to a depth of 60 cm according to ref. [46]. In addition, the soil texture for each soil layer was determined using a hydrometer[47].

Belowground biomass estimation

Fine-root biomass was determined using a core method. Four soil cores (7 cm in diameter) to a depth of 60 cm were collected and separated into four soil layers (that is, 0–15, 15–30, 30–45 and 45–60 cm) in each 10 × 10-m plot. Fine roots (<2 mm) were separated from soils through washing and oven-dried (65 °C for 72 h) for their biomass. Fine roots were further divided into those from woody plants and from grasses on the basis of the stable C isotopic technique using the mass balance equation as presented in equation (2).

Coarse-lateral-root biomass from woody plants was estimated using GPR. GPR profiles were acquired using the Subsurface Interface Radar (SIR) System 4000 with a 1.6-GHz shielded antenna and odometer wheels for position recording (Geophysical Survey Systems, Inc.). Before the survey, the grass layer was carefully removed to avoid any interference in the transmission of electromagnetic energy from antenna to soils (Supplementary Fig. 7). The survey was conducted during the dry season (September to November) of 2018 with soil water content less than 5%. At each 10 × 10-m plot, GPR profiles were collected on a 20-cm grid (Supplementary Fig. 7). If a tree was present on a scanning line, the rest of the GPR profile was obtained from the opposite direction. The topography across all plots was relatively flat, with minimal surface relief (<5 cm). Extra care was taken to ensure the accurate position of each GPR profile with a guide rope and the difference in the length of the GPR profile was less than 1% (that is, 10 cm) of the supposed distance (that is, 10 m). The collection parameters for the SIR-4000 can be found in Supplementary Table 3.

Post-collection data processing was performed with RADAN 7 software (Geophysical Survey Systems, Inc.) using the processing steps shown in Supplementary Fig. 8. Roots were detected as hyperbolic reflectors in the radar profiles. The aim of post-collection processing was to maximize the coherency of root reflectors and differentiate them from the soil background. After basic edits of radar profiles, we applied an exponential gain function to recover amplitude losses from geometric spreading and soil absorption of the radar impulse. Background removal was applied to filter out horizontal reflections resulting from the ground surface, soil horizons and bands of low-frequency noise. A Kirchhoff migration was used to decompose and compact the geometry of hyperbolic reflectors to their source points that are closer to the actual features. The Hilbert transform further collapsed the point-diffraction amplitudes and improved background clutter removal. After these processing techniques, GPR profiles were converted to image files (Supplementary Fig. 8).

To estimate coarse-lateral-root biomass from GPR data, we applied an image-analysis technique to quantify root reflections and used root mass from soil cores for calibration[23,48] (Supplementary Fig. 9). We selected and marked 16 points with a range of root biomass in each 10 × 10-m plot. Eight points were selected on the basis of their distance to the nearest tree and the remainder were identified a priori with GPR to show either high (four points) or low (four points) incidence

of reflections, encompassing the range of root biomass within the plot. Each point was scanned with the 1.6-GHz antenna in both *x* and *y* directions. The location of each point was electronically marked on the radar profile as the antenna was pulled over the centre of the point (Supplementary Fig. 9). After the collection of GPR profiles at each point, a large soil core (15 cm in diameter and 50 cm in length) was used to retrieve coarse roots (>2 mm) to a depth of 50 cm (Supplementary Fig. 9). Roots were oven-dried (65 °C for 72 h) for biomass. GPR profiles were processed and converted to image files. To develop the linear regression equation between root biomass and GPR amplitude, image files were cropped to 15-cm-wide sections in which the antenna was directly over the location of each point. Pixel intensity, a relative measure of how dark or light a pixel is at a greyscale of 0 (black) to 1 (white) (Supplementary Fig. 8), was used to differentiate root reflectors and background in each segment. We used an intensity threshold of >0.8 to delineate roots with minimum illumination of unwanted clutter. We counted pixels with intensity higher than the threshold in each segment to a depth of 50 cm (hereafter, GPR index, pixels with threshold range). For each point, GPR amplitudes from two scanning directions were averaged. Root biomass retrieved from soil cores was then correlated to the GPR index for each EBP string ($n = 48$) to develop regression lines for plot-level biomass estimation (Supplementary Fig. 10). Plot-level image files were sequentially sectioned into 15-cm segments corresponding to the dimensions of the calibration core, hence a 10-m GPR profile yields 67 segments or unique observations. As most of the roots were constrained to the top 60 cm, we calculated the GPR index for each segment to a depth of 60 cm and assigned coordinates to each segment. We then applied the regression line to estimate root biomass for each segment. Ordinary kriging was used to interpolate plot-level coarse-lateral-root biomass on the basis of segment data and their coordinates. The final product was an average of estimates from the *x* and *y* scanning directions (Supplementary Figs. 1–4). The uncertainty of coarse-lateral-root biomass was estimated from the 95% confidence intervals of the regression lines (Extended Data Fig. 5, Supplementary Fig. 10). All image analyses were performed with the package EBImage in R 3.6.1 software[49].

Surface-based GPR readily detects horizontal objects such as lateral roots but is not applicable to estimate the biomass of vertical taproots[23,48,50]. Therefore, taproot biomass was estimated using an allometric equation derived from an empirical study that examined taproot biomass for dominant tree species across the southern Kruger[19]. We then developed a regression relationship between taproot biomass and tree DBH ($R^2 = 0.46$, $P < 0.0001$) (Supplementary Fig. 5), which was subsequently applied to estimate taproot biomass in each 10 × 10-m plot on the basis of the vegetation survey data. The uncertainty of taproot biomass was estimated from the 95% confidence intervals of the regression line (Extended Data Fig. 5, Supplementary Fig. 5).

Aboveground biomass estimation

Woody biomass was estimated using LiDAR. We used a RIEGL VUX-1LR LiDAR unit integrated onto a DJI Matrice 600 Pro unoccupied aerial system to collect high-resolution airborne LiDAR data. We carried out the LiDAR survey during the middle of the wet season (that is, January) of 2020 when vegetation was at full leaf-on stage. The flight altitude was 100 m above ground level, the flight speed was 8 m s^{-1} and the LiDAR scan rate was 78.1 lines s^{-1} (see Supplementary Table 4 for other parameter settings). The unoccupied aerial system maintained consistent elevation above the ground by using 30 × 30-m elevational data from the Shuttle Radar Topography Mission to adjust flight altitude in real time during the survey. All treatments in each string were surveyed with transects of identical heading to decrease the probability of introducing confounding variables and remote-sensing artefacts created by differing survey methodologies or LiDAR scan directions.

LiDAR is an active-remote-sensing technique that characterizes vegetation structure in three-dimensional space across large spatial extents. LiDAR sensors emit coherent laser pulses and measure the distance to the targets from the time delay of the returned laser pulses to the sensor. The location of each laser return is presented as a 'point cloud', which contains *x*, *y* and *z* location data from an embedded Global Positioning System–inertial measurement unit in the LiDAR system. Therefore, LiDAR data consist of a larger number of georeferenced points with elevation estimates and other radiometric attributes of the vegetation. We processed the LiDAR data using Terrasolid software (Terrasolid Ltd.). First, LiDAR data from all the flight lines were denoised, ground-classified and matched together with an accuracy of around 2–3 cm. After noise-point removal, the average point density across all the sites was about 150 points per m^2. Points that penetrated the vegetation canopy and reached the ground surface were used to interpolate a digital terrain model. Then, all first-return points were compared with a triangulated irregular network model of the ground to calculate the height above the ground surface for each point. A gridded canopy height model (CHM) was derived at a 10-cm resolution by filling each cell with the maximum height above ground of any first-return points within the cell.

We used an object-based image-segmentation approach to estimate the aboveground woody biomass from the LiDAR-derived CHM[21]. The CHM was used to identify treetops using an algorithm based on a local maximum filter[51]; a dynamic moving-window approach was used to scan the CHM and if a given cell was found to be the highest within the window, it was tagged as a treetop. The height of each treetop was retrieved from the CHM. The algorithm was trained to ensure that trees with height > 5 m were accurately detected, which contribute most to the aboveground woody biomass. On the basis of this algorithm, the LiDAR-derived stem density (>5 m) was highly correlated with the field-measured stem density[52] ($R^2 = 0.90$) (Extended Data Fig. 8a). Next, tree crowns were segmented on the basis of a watershed algorithm guided by the locations of the treetops[53]. The area of each tree crown was calculated as the projection of the outlined crown on the ground surface. After computing the height and the crown area, a regression model developed specifically for savanna trees in Kruger was applied to generate aboveground biomass per individual tree[21]:

$$\log_{10}(m) = \beta_0 + \beta_1 * \log_{10}(A_{\mathrm{obj}}) + \beta_2 * (\log_{10}(A_{\mathrm{obj}}))^2 + \beta_3 * \log_{10}(H_{\mathrm{obj}}) \quad (3)$$

in which m is the tree biomass (kg), A_{obj} is the object-projected crown area (m^2) and H_{obj} is the tree height (m). β_0, β_1, β_2 and β_3 are least-squares regression coefficients and are estimated as 0.115, 0.161, 0.252 and 1.73, respectively. In this study, we set a minimum height of 0.5 m to ensure that we detected only woody plants. We used the coordinates of the centre of each GPR plot (that is, 10 × 10 m) to set a buffer of radius 15 m to compute the aboveground woody biomass of each plot (Supplementary Figs. 1–4). The 30-m-diameter LiDAR plot allows for small location errors of the GPR plot and also matches the area obtained for developing the regression model as presented in equation (3) (ref. [21]). Only woody plants with their centroids within the buffer were included. In addition, to cross-validate the object-based LiDAR biomass estimation, we also estimated aboveground woody biomass using species-specific allometric equations on the basis of DBH[54], as well as plot-averaged pixel-based LiDAR calibration[21] (see Extended Data Fig. 8 for more details). However, we chose to report object-based LiDAR biomass estimation in the main text, because the object-based method is better suited to open-canopy systems and provides a more accurate proxy for measured woody biomass than allometric estimates[21]. All analyses were performed with the ForestTools[55] and raster[56] packages in R 3.6.1 software.

Grass biomass was estimated from the long-term monitoring of grass fuel loads for the EBP trial in Kruger (Extended Data Fig. 4) using a disc pasture meter calibrated for savannas in Kruger[18]. Before each fire, 100 points in each treatment were sampled to obtain an estimate of the mean fuel load. However, because the grass fuel load for the unburned treatments was not available, we used disc pasture meter data from a wet-season fire treatment (that is, burning in April for every two years),

in which fires rarely successfully ignite and where tree cover is comparable with that of the unburned treatment, as a surrogate. To validate this assumption, we compared grass-biomass estimates on the basis of field measurements with grass canopy height estimated from the LiDAR CHM described above (averaging canopy height for all pixels without a 'tree' of height > 0.5 m); we found a close correspondence between estimates (R^2 = 0.38; see Extended Data Fig. 4), suggesting that the April B2 treatment provides a reasonable grass-biomass proxy for the unburned treatment. Grass biomass for each fire treatment across the Pretoriuskop landscape was estimated by averaging available data from 1982 to 2010, to capture interannual variation in grass-biomass accumulation, which can be substantial[24].

Data analyses

We used the depth distribution of the GPR index (that is, pixel counts above the threshold) in percentage as an indicator to examine how changes in fire frequency would affect root biomass investment throughout the soil profile. We calculated the depth (cm) at which the cumulative GPR amplitude reached 50% for each fire treatment in each string to facilitate the comparison. Vegetation biomass was converted to C storage using a factor of 0.5, which is recommended by the Intergovernmental Panel on Climate Change (IPCC)[57]. The unit of ecosystem C storage was presented as Mg C ha^{-1}.

We fitted linear mixed models using string as a random intercept and fire treatment as the fixed term to detect the significance of measured parameters. The package lmerTest[58], which approximates the degrees of freedom using Satterthwaite's method, was used to evaluate the significance of terms. We also fitted our data to ranked mixed models, in which fire treatments were ranked from low to high frequency. The results were generally consistent across the two approaches (see Extended Data Table 1). In addition, we used linear mixed models to examine the influence of tree cover and/or soil sand content on SOC storage, C_3-derived and C_4-derived SOC storage, belowground to aboveground C storage and other parameters. The marginal R^2 was calculated accordingly. All data analyses were performed using R 3.6.1 software.

Data and code availability

Data and code are available in the Dryad Digital Repository: https://doi.org/10.5061/dryad.pg4f4qrr5. Source data are provided with this paper.

43. Venter F. A. *Classification of Land for Management Planning in the Kruger National Park*. PhD thesis, Univ. South Africa (1990).
44. Biggs, R., Biggs, H. C., Dunne, T. T., Govender, N. & Potgieter, A. L. F. Experimental burn plot trial in the Kruger National Park: history, experimental design and suggestions for data analysis. *Koedoe* **46**, 15 (2003).
45. Codron, J. et al. Taxonomic, anatomical, and spatio-temporal variations in the stable carbon and nitrogen isotopic compositions of plants from an African savanna. *J. Archaeol. Sci.* **32**, 1757–1772 (2005).
46. Zhou, Y., Boutton, T. W. & Ben Wu, X. Soil carbon response to woody plant encroachment: importance of spatial heterogeneity and deep soil storage. *J. Ecol.* **105**, 1738–1749 (2017).
47. Sheldrick B. & Wang C. In *Soil Sampling and Methods of Analysis* (ed. Carter, M. R.) 499–511 (CRC Press, 1993).
48. Butnor, J. R. et al. Surface-based GPR underestimates below-stump root biomass. *Plant Soil* **402**, 47–62 (2016).
49. Pau, G., Fuchs, F., Sklyar, O., Boutros, M. & Huber, W. EBImage—an R package for image processing with applications to cellular phenotypes. *Bioinformatics* **26**, 979–981 (2010).
50. Hirano, Y. et al. Limiting factors in the detection of tree roots using ground-penetrating radar. *Plant Soil* **319**, 15–24 (2009).
51. Popescu, S. C. & Wynne, R. H. Seeing the trees in the forest. *Photogramm. Eng. Remote Sensing* **70**, 589–604 (2004).
52. Case, M. F., Wigley-Coetsee, C., Nzima, N., Scogings, P. F. & Staver, A. C. Severe drought limits trees in a semi-arid savanna. *Ecology* **100**, e02842 (2019).
53. Beucher S. & Meyer F. In *Mathematical Morphology in Image Processing* (ed. Dougherty, E. R.) 433–481 (CRC Press, 1993).
54. Nickless, A., Scholes, R. J. & Archibald, S. A method for calculating the variance and confidence intervals for tree biomass estimates obtained from allometric equations. *S. Afr. J. Sci.* **107**, 1–10 (2011).
55. Plowright A. & Roussel J.-R. ForestTools: analyzing remotely sensed forest data. R package version 0.2.1. https://CRAN.R-project.org/package=ForestTools (2020).
56. Hijmans R. J. raster: geographic data analysis and modeling. R package version 3.3-7. https://CRAN.R-project.org/package=raster (2020).
57. Penman J. et al. (eds) *Good Practice Guidance for Land Use, Land-Use Change and Forestry* (Intergovernmental Panel on Climate Change, 2003).
58. Kuznetsova, A., Brockhoff, P. & Christensen, R. lmerTest package: tests in linear mixed effects models. *J. Stat. Softw.* **82**, 1–26 (2017).

Acknowledgements We gratefully acknowledge the logistical support provided by South African National Parks staff in Kruger National Park. Y.Z. was supported by a G. Evelyn Hutchinson Environmental Postdoctoral Fellowship from the Yale Institute for Biospheric Studies, A.C.S. was partially supported by a grant from the United States National Science Foundation (NSF MSB-1802453) and by funding from Yale University, J.S., P.B.B., E.G.H. and A.B.D. from Harvard University, and J.R.B. from the USDA Forest Service, Southern Research Station.

Author contributions Conceptualization: Y.Z. and A.C.S.; methodology: Y.Z., J.S., J.R.B., P.B.B., A.B.D. and A.C.S.; investigation: Y.Z., C.C., M.F.C., E.G.H., A.B.D. and A.C.S.; visualization: Y.Z. and A.C.S.; funding acquisition: A.B.D. and A.C.S.; project administration: A.B.D. and A.C.S.; supervision: A.B.D. and A.C.S.; writing — original draft: Y.Z. and A.C.S.; writing — review and editing: Y.Z., J.S., J.R.B., C.C., P.B.B., M.F.C., E.G.H., A.B.D. and A.C.S.

Competing interests The authors declare no competing interests.

Additional information

Supplementary information The online version contains supplementary material available at https://doi.org/10.1038/s41586-022-04438-1.

Correspondence and requests for materials should be addressed to Yong Zhou or A. Carla Staver.

Peer review information *Nature* thanks Sebastian Dötterl, Niall Hanan and Douglas Morton for their contribution to the peer review of this work. Peer reviewer reports are available.

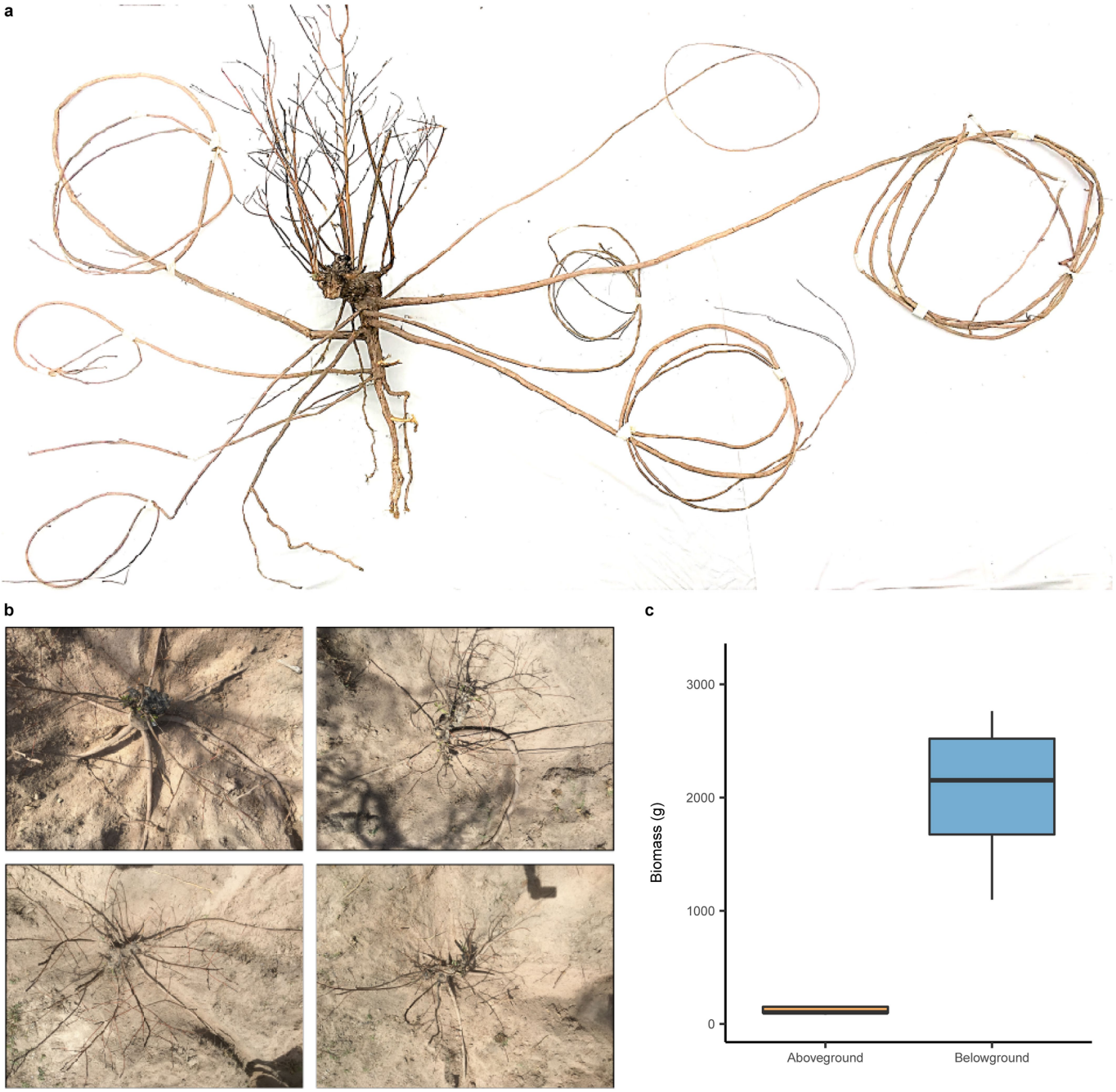

Extended Data Fig. 1 | An example showing belowground to aboveground biomass allocation for resprouting *Terminalia sericea*. **a**, **b**, Five *T. sericea* individuals that have experienced annual burning were excavated in the Pretoriuskop landscape in Kruger National Park, South Africa. **c**, The difference between aboveground and belowground biomass and the ratio of belowground to aboveground biomass was 19.5. The box plots show medians (that is, 50th percentile), 25th and 75th percentiles, and the approximate 95% confidence interval for five replicates.

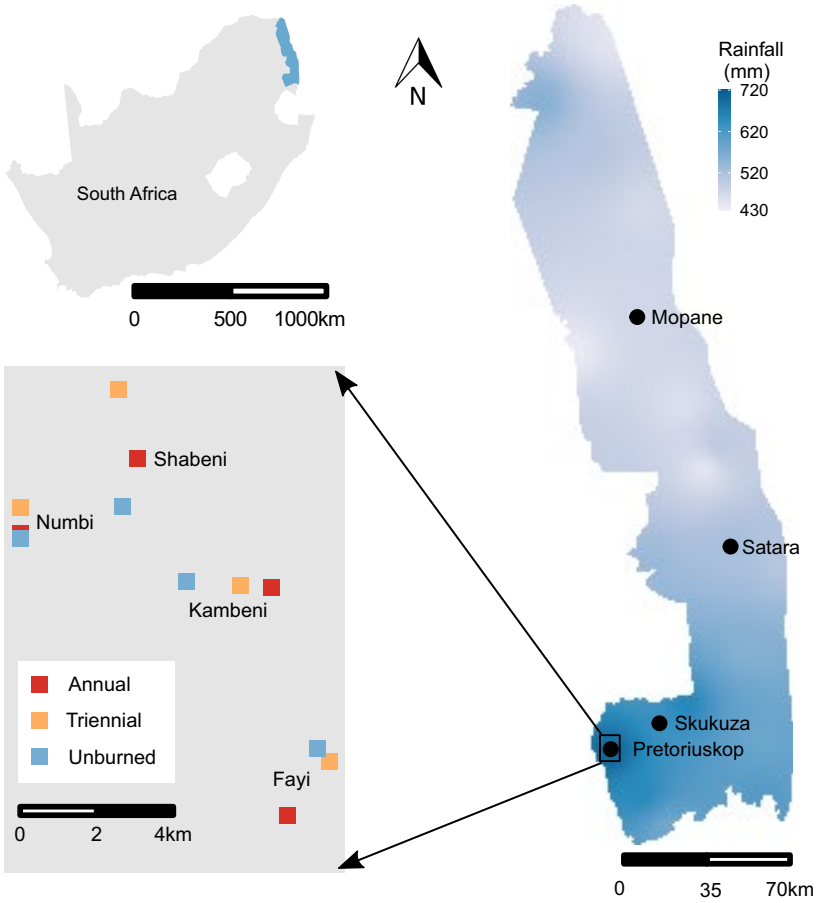

Extended Data Fig. 2 | Maps showing the study site. Maps showing the locations of different fire treatments (that is, annual, triennial and unburned) examined in this study and located in each string (Fayi, Kambeni, Numbi and Shabeni) across the Pretoriuskop landscape at Kruger National Park, South Africa. Base map for South Africa modified from Natural Earth.

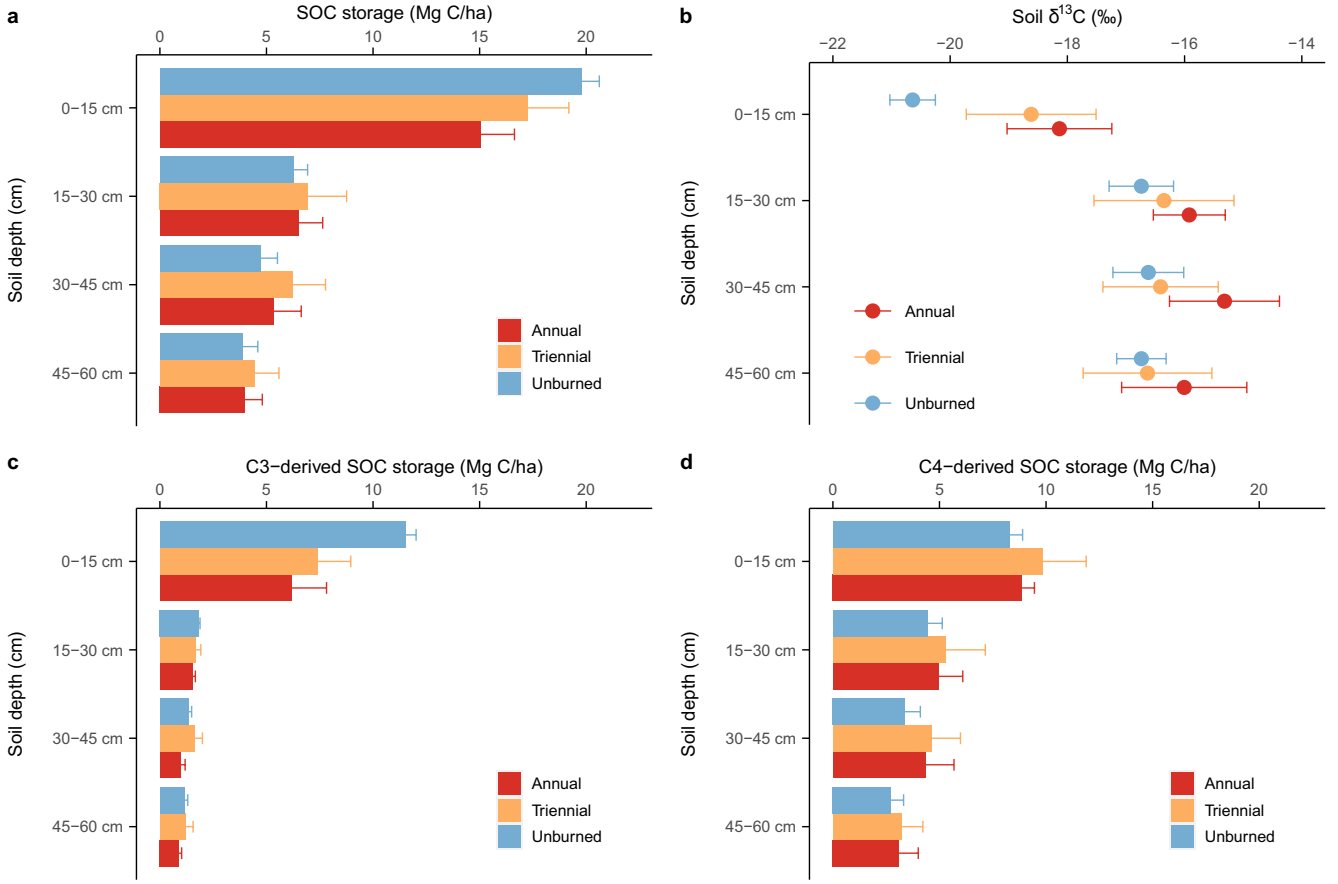

Extended Data Fig. 3 | Changes in SOC storage and soil $\delta^{13}C$ across different fire treatments throughout the 60-cm soil column. Effects of fire treatments on total SOC storage (Mg C ha^{-1}) (**a**), soil $\delta^{13}C$ (‰) (**b**), C_3-derived SOC storage (that is, from woody plants) (Mg C ha^{-1}) (**c**) and C_4-derived SOC storage (that is, from grasses) (Mg C ha^{-1}) (**d**). Values are mean ± standard errors ($n = 4$).

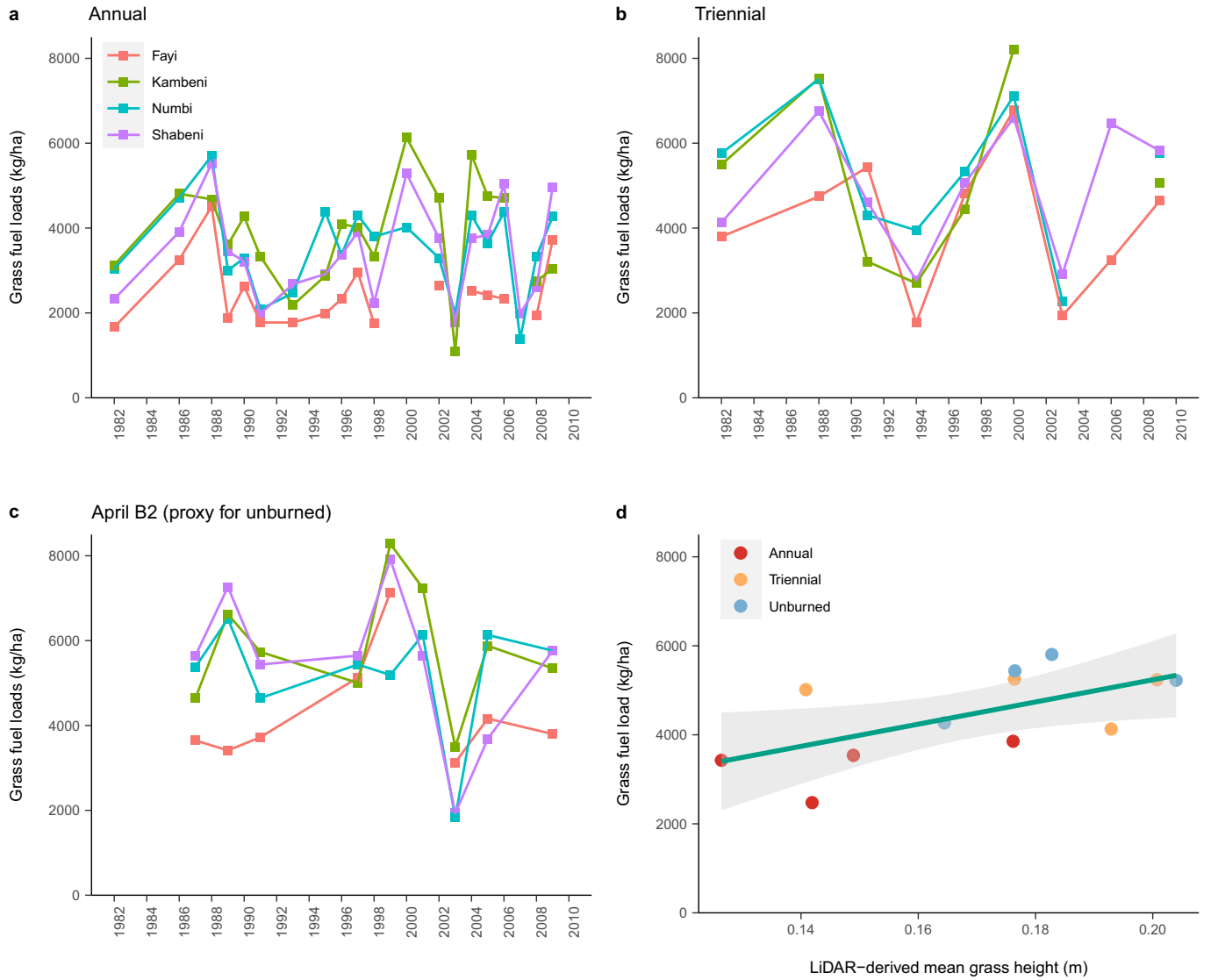

Extended Data Fig. 4 | Long-term monitoring of grass fuel loads and their correlation to LiDAR-derived mean grass height. a–**c**, Grass fuel loads (kg ha^{-1}) for annual (**a**), triennial (**b**) and April B2 (that is, burning in April for every two years, as a proxy for unburned) (**c**) treatments from 1982 to 2009 for different strings at the Pretoriuskop landscape in Kruger National Park, South Africa. Disconnected lines indicate missing data for specific years. **d**, The correlation between averaged grass fuel loads from 1982 to 2009 and LiDAR-derived mean grass heights (m) ($R^2 = 0.38$, $P = 0.03$). The mean grass height was calculated by averaging heights of pixels that range from 0.05 to 0.5 m in the CHM derived from LiDAR. Please note especially that, in panel **d**, LiDAR-derived mean grass height was estimated from the unburned treatment itself, but that field-estimated grass fuel load was estimated from the April B2 treatment as a proxy (as grass fuel load is not routinely measured for the unburned treatment).

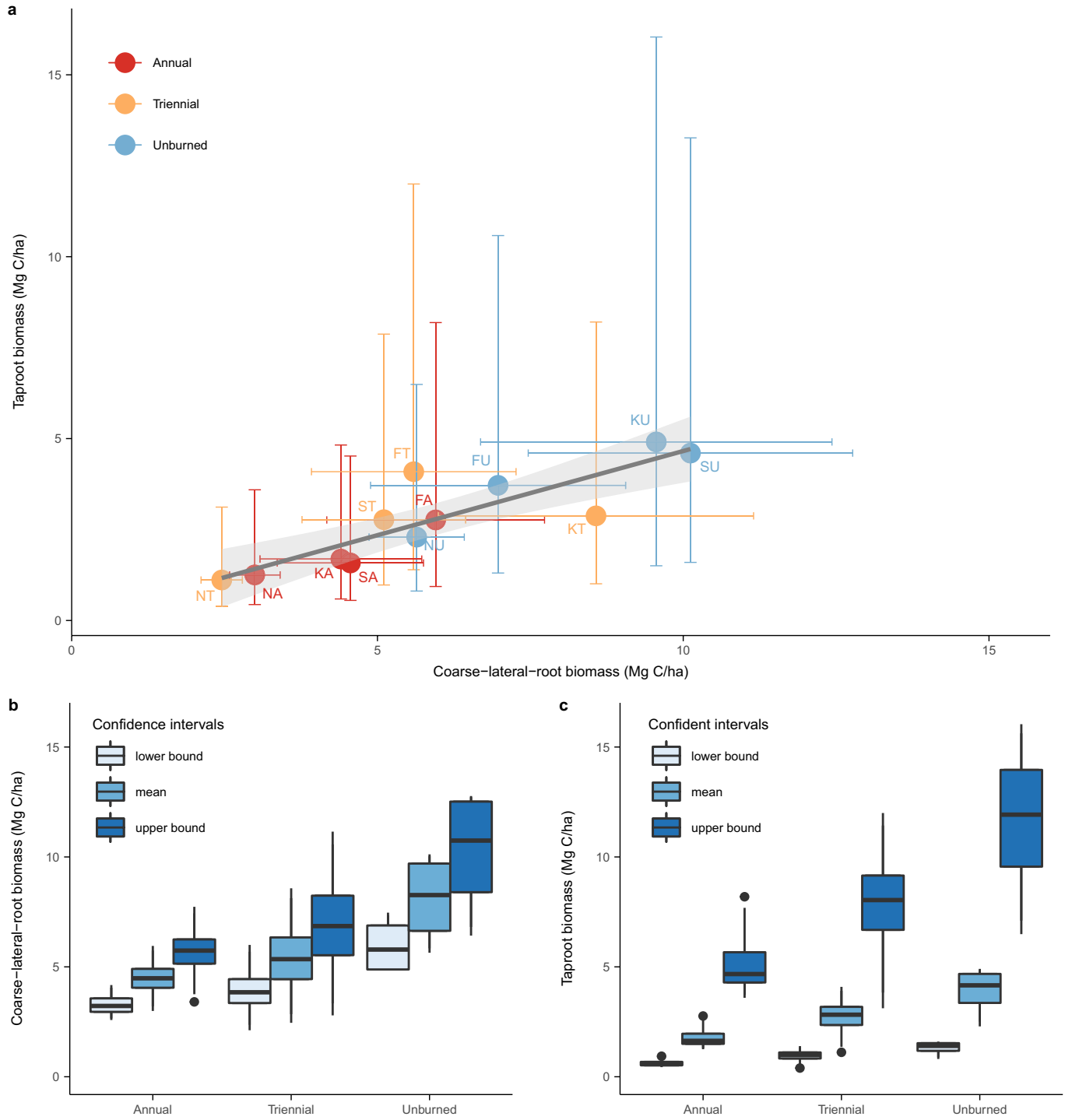

Extended Data Fig. 5 | The uncertainty of coarse lateral and taproot biomass estimates. a, The uncertainty of coarse lateral and taproot biomass for each treatment replicate. Error bars indicate the 95% confidence interval for coarse lateral and taproot biomass estimates derived from fitting regression lines (see Supplementary Figs. 5 and 10). Coarse-lateral-root biomass estimates were significantly correlated with taproot biomass estimates ($R^2 = 0.75$, $P < 0.001$). Letters F, K, N and S indicate Fayi, Kambeni, Numbi and Shabeni strings at the Pretoriuskop landscape in Kruger National Park, South Africa; letters A, T and U indicate annual, triennial and unburned treatments. **b**, **c** The uncertainty of (that is, lower bound, mean and upper bound) coarse lateral and taproot biomass across different fire treatments. The box plots show medians (that is, 50th percentile), 25th and 75th percentiles, and the 95% confidence interval for four replicates. Points in **b** and **c** indicate outliers.

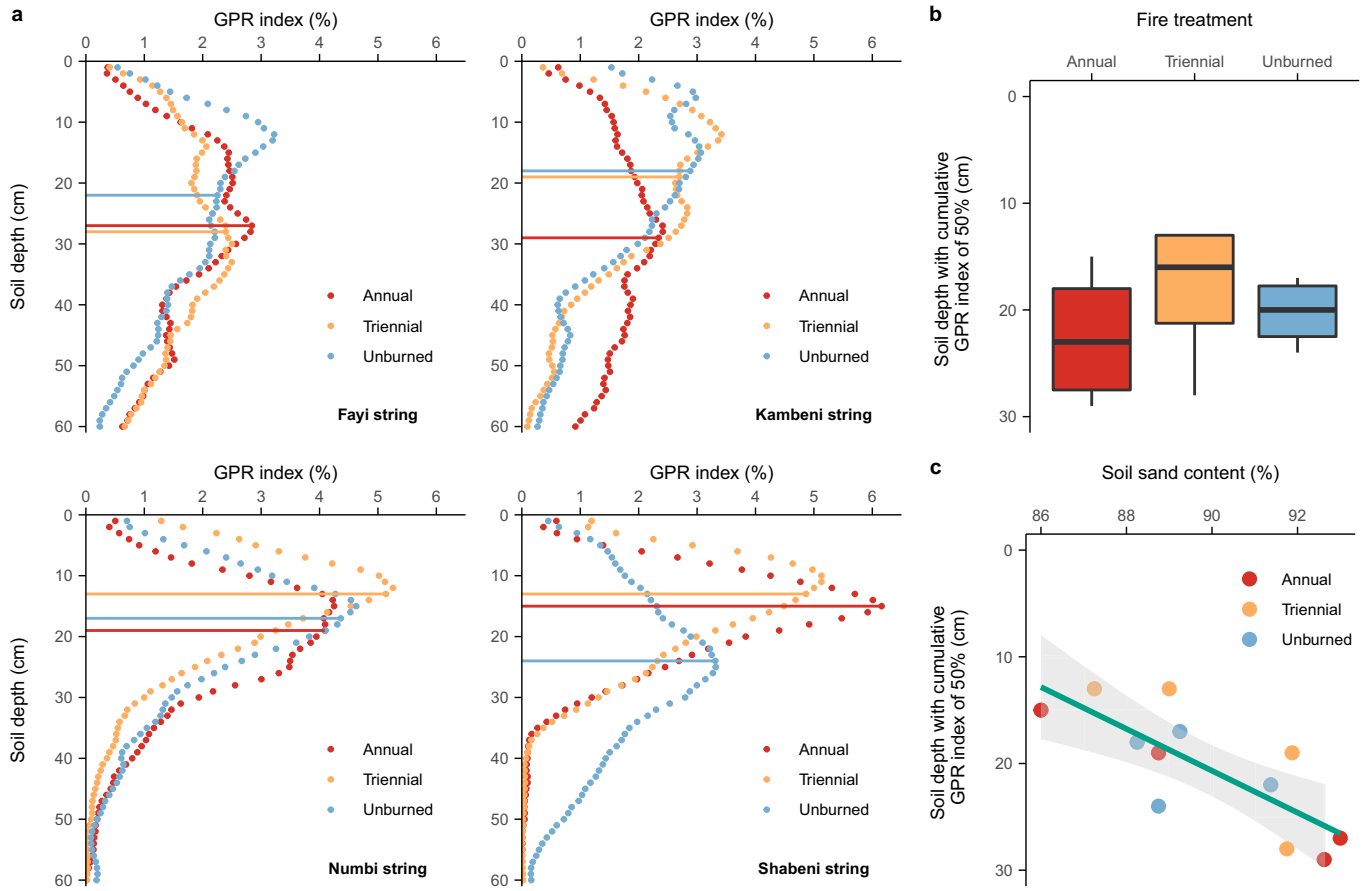

Extended Data Fig. 6 | Depth distribution of coarse-lateral-root biomass across fire treatments and soil sand content. a, Depth distribution of the GPR index (% in the number of pixels above the threshold for root detections) as an indicator of coarse-lateral-root biomass allocation throughout the soil column across different fire treatments at each string. Horizontal lines indicate the depth (cm) at which the GPR index reaches 50% of the total detections in the 60-cm soil column. **b**, Effects of fire treatment on the depth distribution of coarse-lateral-root biomass ($P = 0.51$). The box plots show medians (that is, 50th percentile), 25th and 75th percentiles, and the 95% confidence interval for four replicates. **c**, The correlation between soil sand content (%) and depth distribution of coarse-lateral-root biomass ($R^2 = 0.61$, $P = 0.003$). The regression line indicates the significant linear fit and the shaded bands illustrate the 95% confidence interval of the linear fit.

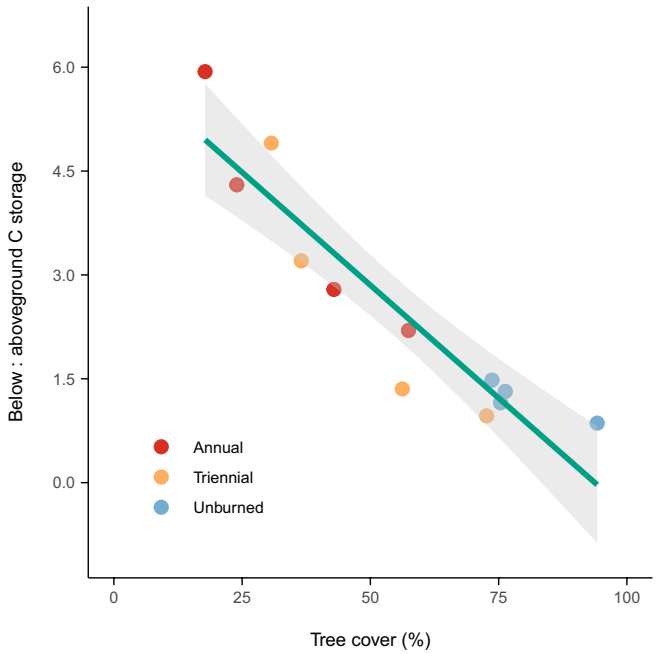

Extended Data Fig. 7 | The correlation between ratio of belowground to aboveground carbon storage and tree cover (%) (R^2 = 0.83, P < 0.0001). The regression line indicates the significant linear fit and the shaded bands illustrate the 95% confidence interval of the linear fit.

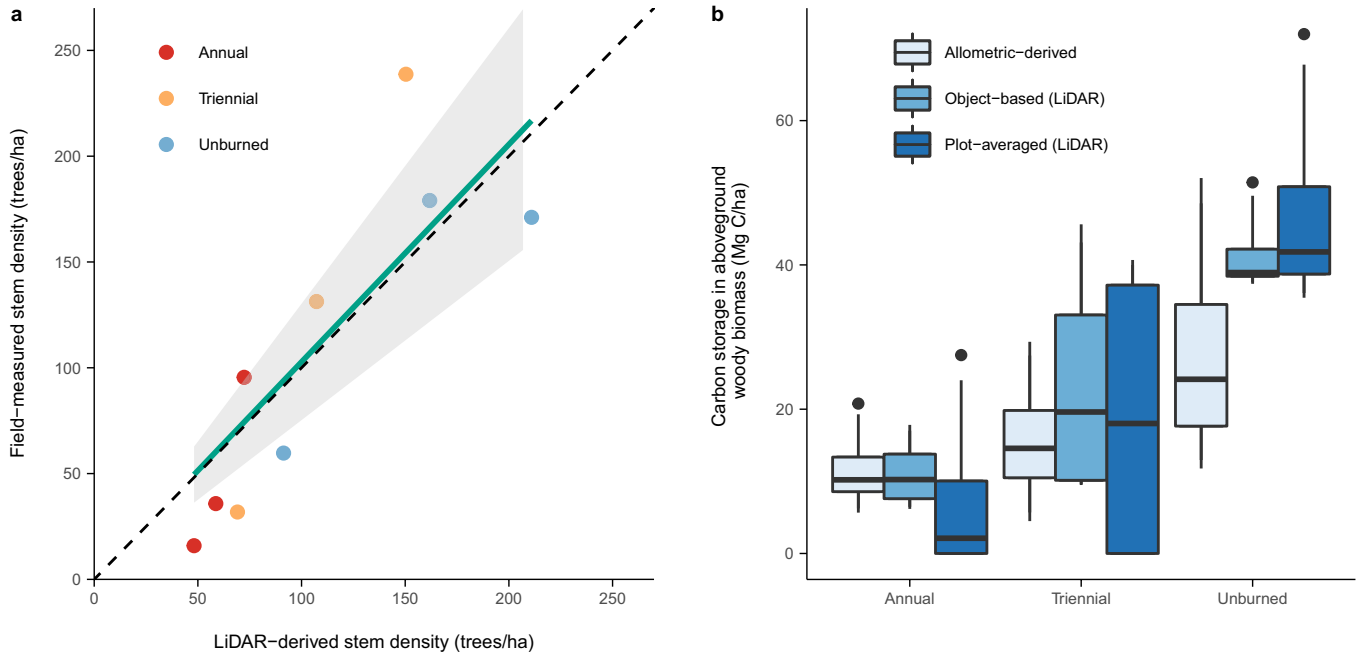

Extended Data Fig. 8 | The validation of the object-based method to estimate aboveground woody biomass. a, The correlation between LiDAR-derived stem density for trees with height > 5m (trees ha^{-1}) and field-measured stem density (trees ha^{-1}). The field-measured stem density was from ref. [52], which surveyed tree heights in eight 10-m-radius plots at each annual, triennial and unburned treatment in Kambeni, Numbi and Shabeni strings at the Pretoriuskop landscape in Kruger National Park, South Africa. The regression line indicates the significant linear fit and the shaded bands illustrate the 95% confidence interval of the linear fit. The dashed line indicates the 1:1 line. **b**, Differences in aboveground woody biomass between allometric-derived, object-based and plot-averaged estimates. The allometric-derived biomass estimation was on the basis of species-specific allometric equations developed in ref. [54], which predict aboveground woody biomass from DBH. This estimation was calculated for trees with DBH > 5 cm in each 10 × 10-m plot. The plot-averaged LiDAR biomass was estimated using an allometric equation derived from on-the-ground plot-level sampling relating aboveground woody biomass to LiDAR-derived canopy height and canopy area (aboveground woody biomass = −11.5 + 25.8 * canopy height * canopy area); please refer to ref. [21] for more details. The canopy height and canopy area were averaged across pixels with height > 0.5 m in each 30-m-radius plot. The box plots show medians (that is, 50th percentile), 25th and 75th percentiles, and the 95% confidence interval for four replicates. Points in **b** indicate outliers.

Extended Data Table 1 | Results comparing the relative effect of different fire treatments on each component of ecosystem carbon storage from linear mixed-effects models using fire treatments as the fixed effect and string as a random effect

	Linear mixed model			*Ranked mixed model*		
Response variable	df	*F*	*p*	*df*	*t*	*p*
Total aboveground biomass	2, 6	10.51	0.011	6	4.57	0.0038
Aboveground woody biomass	2, 6	9.90	0.013	6	4.43	0.0044
Aboveground grass biomass	2, 6	210.44	< 0.001	6	19.01	< 0.001
Total belowground biomass	2, 6	8.67	0.017	6	3.84	0.0086
Woody fine root biomass	2, 6	4.31	0.069	6	2.51	0.046
Grass fine root biomass	2, 6	2.11	0.20	6	-1.81	0.12
Woody lateral root biomass	2, 6	10.62	0.011	6	4.25	0.0054
Woody tap root biomass	2, 6	8.04	0.020	6	4.00	0.0071
Total SOC storage	2, 6	0.82	0.48	6	1.08	0.32
C3-derived SOC storage	2, 6	8.48	0.018	6	4.07	0.0065
C4-derived SOC storage	2, 6	0.80	0.49	6	-0.75	0.48
Whole-ecosystem C storage	2, 6	18.7	0.0026	6	6.10	0.0009
Woody root-to-shoot ratio	2, 6	2.75	0.14	6	-12.30	0.061
Below-to-aboveground C storage ratio	2, 6	4.74	0.058	6	-3.08	0.022

Results from linear mixed models were also compared with results from ranked mixed model using ranked fire treatments as the fixed effect and string as a random effect.